ISSN 1063-7761, Journal of Experimental and Theoretical Physics, 2012, Vol. 114, No. 2, pp. 259–272. © Pleiades Publishing, Inc., 2012.
Original Russian Text © A.A. Demidov, I.A. Gudim, E.V. Eremin, 2012, published in Zhurnal Eksperimental'noi i Teoreticheskoi Fiziki, 2012, Vol. 141, No. 2, pp. 294–309.

ORDER, DISORDER, AND PHASE TRANSITION IN CONDENSED SYSTEM

Magnetic Phase Transitions in $Nd_{1-x}Dy_xFe_3(BO_3)_4$ Ferroborates

A. A. Demidov[a], I. A. Gudim[b], and E. V. Eremin[b]

[a] *Bryansk State Technical University, Bryansk, 241035 Russia*

[b] *Kirensky Institute of Physics, Siberian Branch, Russian Academy of Sciences, Krasnoyarsk, 660038 Russia*

e-mail: demandr@yandex.ru

Received February 26, 2011

Abstract—The magnetic properties of ferroborate single crystals with substituted compositions $Nd_{1-x}Dy_xFe_3(BO_3)_4$ ($x = 0.15, 0.25$) with competing exchange Nd–Fe and Dy–Fe interactions are investigated. For each composition, we observed a spontaneous spin-reorientation transition from the easy-axis to the easy-plane state and step anomalies on the magnetization curves for the spin-flop transition induced by a magnetic field $\mathbf{B} \parallel \mathbf{c}$. The measured parameters and effects are interpreted using a unified theoretical approach based on the molecular field approximation and on calculations performed in the crystal-field model for the rare-earth ion. The experimental temperature dependences of the initial magnetic susceptibility from $T = 2$ K to $T = 300$ K, anomalies on the magnetization curves for $\mathbf{B} \parallel \mathbf{c}$ in fields up to 1.8 T, and their evolution with temperature, as well as temperature and field dependences of magnetization in fields up to 9 T are described. In the interpretation of experimental data, the crystal-field parameters in trigonal symmetry for the rare-earth subsystem are determined, as well as the parameters of Nd–Fe and Dy–Fe exchange interactions.

DOI: 10.1134/S1063776111160023

1. INTRODUCTION

Rare-earth ferroborates $RFe_3(BO_3)_4$ are of considerable interest for the physics of magnetic phenomena as *f–d* compounds with a specific interaction between the rare-earth and iron subsystems. It has been established that $RFe_3(BO_3)_4$ compounds belong to the class of multiferroics in which elastic, magnetic, and electric order parameters coexist [1, 2]. The main elements of the crystal structure of rare-earth ferroborates (space group $R32$) are spiral chains of FeO_6 octahedrons contacting along the edge and oriented along the c axis [3]. The bonds between Fe^{3+} ions along the chain and between the chains are such that the antiferromagnetic interaction in a chain is stronger than the interaction between the chains. The iron subsystem in $RFe_3(BO_3)_4$ becomes ordered at Néel temperatures T_N on the order of 30–40 K. The rare-earth subsystem is magnetized by the *f–d* interaction and makes a significant contribution to the magnetic anisotropy and orientation of the magnetic moments. Since ferroborates with different R ions have different magnetic structures, the role of the rare-earth subsystem in the formation of the magnetic structure can be determined in the study of magnetic characteristics and phase transitions using tested theoretical models (e.g., the crystal-field model for the R ion in a compound). Ferroborates can be easy-axis (with magnetic moments of R and Fe oriented along the c axis of the crystal) or easy-plane (with magnetic moments of R and Fe lying in the ab plane of the crystal) compounds, or can spontaneously pass from the easy-axis to the easy-plane state as in $GdFe_3(BO_3)_4$ and $HoFe_3(BO_3)_4$.

The first results of analysis of substituted ferroborates $R_{1-x}R'_xFe_3(BO_3)_4$ were reported in 2008–2009 [4–8]. The affiliation of $R_{1-x}R'_xFe_3(BO_3)_4$ to multiferroics is being established at present [4, 6–8]. In the presence of competing R–Fe and R'–Fe interactions in $R_{1-x}R'_xFe_3(BO_3)_4$, effects associated that are with the competition of the contributions can appear (e.g., spontaneous reorientation transitions between the easy-axis and easy-plane states [4–8]).

In $NdFe_3(BO_3)_4$, the magnetic moments of the neodymium and iron subsystems lie in the basal ab plane [2, 9]; the magnetic moments of Dy and Fe in $DyFe_3(BO_3)_4$ are oriented along the trigonal c axis and the spin-flop transition takes place for $\mathbf{B} \parallel \mathbf{c}$ [10]. Thus, due to the competition of different contributions from the Nd^{3+} and Dy^{3+} ions to the magnetic anisotropy of $Nd_{1-x}Dy_xFe_3(BO_3)_4$, spontaneous and magnetic field-induced spin-reorientation transitions from the c axis to the ab plane can occur [4, 5]. For $Nd_{0.75}Dy_{0.25}Fe_3(BO_3)_4$ [4, 7] and $Nd_{1-x}Dy_xFe_3(BO_3)_4$ ($x = 0.1, 0.25$) [5], anomalies in the behavior of magnetic susceptibility, magnetization, spontaneous electric polarization, and magnetostriction were observed; $H–T$ diagrams of possible magnetic phases were constructed as well.

However, some fundamental questions for $Nd_{1-x}Dy_xFe_3(BO_3)_4$ ferroborates remain unanswered. For example, in the experimental data available on

$Nd_{0.75}Dy_{0.25}Fe_3(BO_3)_4$, anomalies on magnetization curves for $\mathbf{B} \parallel \mathbf{c}$ do not coincide [4, 5]. As a result, the $H-T$ diagrams constructed for possible magnetic phases are different and various opinions about the origin and mechanisms of the observed anomalies exist [4, 5, 7]. It was shown in [4] that the antiferromagnetic state of $Nd_{0.75}Dy_{0.25}Fe_3(BO_3)_4$ below $T_N \approx 32$ K is an easy-plane state, and the anomaly of the magnetic susceptibility curves near $T \approx 25$ K is due to a spin-reorientation transition from the easy-plane to the easy-axis state. Anomalies were observed in the behavior of magnetization, spontaneous electric polarization, and magnetostriction upon the spin-flop transition induced by magnetic field $\mathbf{B} \parallel \mathbf{c}$ and the $H-T$ diagram was constructed. It was found in [5] that the temperature dependence of the magnetization exhibits two singularities at $T_1 \approx 16$ K and $T_2 \approx 24$ K for $Nd_{0.75}Dy_{0.25}Fe_3(BO_3)_4$ and one singularity at $T \approx 8$ K for $Nd_{0.9}Dy_{0.1}Fe_3(BO_3)_4$. Step anomalies on magnetization curves $M_c(B)$ for $Nd_{0.75}Dy_{0.25}Fe_3(BO_3)_4$ were also observed in the vicinity of the spin-flop transition field; only one anomaly was detected on analogous curves in [4]. In [6], the elastic properties of $Nd_{0.75}Dy_{0.25}Fe_3(BO_3)_4$ were studied by the ultrasound method. Singularities in the temperature and magnetic-field dependences of the velocity and absorption of transverse sound were investigated. These singularities are interpreted as manifestations of magnetic phase transitions. A version of the low-temperature part of the $H-T$ phase diagram that differs from the results obtained in [4] was produced.

This study is devoted to experimental and theoretical investigation of the low-temperature dependences of magnetic phase transitions in $Nd_{1-x}Dy_xFe_3(BO_3)_4$ ($x = 0.15, 0.25$), to comparison of the experimental data with the results of calculations performed within a unified theoretical approach, and to the determination of parameters of compounds.

2. EXPERIMENTAL

Single crystals were grown from solutions–melts based on bismuth trimolybdate 75 wt % $\{Bi_2Mo_3O_{12} + 3B_2O_3 + 0.6[(1-x)Nd_2O_3 + xDy_2O_3]\}$ + 25 wt % $Nd_{1-x}Dy_xFe_3(BO_3)_4$ in accordance with the technique described in detail in [5]. The crystals were grown in the solution–melt with a mass of 300 g simultaneously on four seeds with a volume of approximately 1 mm^3 under identical hydrodynamic conditions. The crystal holder was reversibly rotated at a velocity of 30 rpm with a period of 1 min. The supercooling corresponded to an increase in height of less than 1 mm/day. After the end of growth, the crystal holder was lifted above the solution–melt; the crystals were then cooled to room temperature with a switched-off oven. The thus-grown crystals with a height of 6–10 mm had a small triangular {0001} pinacoid face, which was perpendicular to the C_3 axis. Samples with the required orientation were prepared in accordance with the crystal morphology. The crystals had a good optical quality and did not contain visible defects. The neodymium and dysprosium concentrations in a crystal were determined using X-ray spectral fluorescent analysis. Magnetic measurements were taken on a Physical Properties Measurement System (Quantum Design) in a temperature interval of 2–300 K in magnetic fields up to 9 T.

3. COMPUTATIONAL TECHNIQUE

The magnetic properties of $Nd_{1-x}Dy_xFe_3(BO_3)_4$ ferroborates are determined by both magnetic subsystems, viz., the rare-earth (neodymium and dysprosium) subsystem and the iron subsystem, which interact with each other. The interaction within the R subsystem can be disregarded because none of rare-earth ferroborates [3, 11] or rare-earth alumoborates isostructural to them [12] has its own ordering in the R subsystem. The iron subsystem can be treated as an aggregate of two antiferromagnetic sublattices. The R subsystem magnetized due to the f–d interaction can also be represented in the form of two sublattices.

In our calculations, we used the theoretical approach that was successfully employed for pure ferroborates $RFe_3(BO_3)_4$ with R = Tb ([13–15], Nd [9], Dy [10, 16], Pr [17], Er [18, 19], and Ho [20] and adapted to ferroborates with substituted compositions $Nd_{1-x}Dy_xFe_3(BO_3)_4$ with competing Nd–Fe and Dy–Fe exchange interactions. This theoretical approach is based on the crystal field model for the rare-earth subsystem and on the molecular field approximation.

Proceeding from the magnetic structure and the hierarchy of the interaction of $Nd_{1-x}Dy_xFe_3(BO_3)_4$ in magnetic field $\mathbf{B}$, the effective Hamiltonians of the R/Fe ion of the ith ($i = 1, 2$) sublattice can be written in the form

$$\mathcal{H}_i(\mathrm{Nd}) = \mathcal{H}_i^{\mathrm{CF(Nd)}} - g_J^{\mathrm{Nd}}\mu_B\mathbf{J}_i^{\mathrm{Nd}}[\mathbf{B} + \lambda_{\mathrm{fd}}^{\mathrm{Nd}}\mathbf{M}_i^{\mathrm{Fe}}], \quad (1)$$

$$\mathcal{H}_i(\mathrm{Dy}) = \mathcal{H}_i^{\mathrm{CF(Dy)}} - g_J^{\mathrm{Dy}}\mu_B\mathbf{J}_i^{\mathrm{Dy}}[\mathbf{B} + \lambda_{\mathrm{fd}}^{\mathrm{Dy}}\mathbf{M}_i^{\mathrm{Fe}}], \quad (2)$$

$$\mathcal{H}_i(\mathrm{Fe}) = -g_S\mu_B\mathbf{S}_i[\mathbf{B} + \lambda\mathbf{M}_j^{\mathrm{Fe}} + (1-x)\lambda_{\mathrm{fd}}^{\mathrm{Nd}}\mathbf{m}_i^{\mathrm{Nd}} + x\lambda_{\mathrm{fd}}^{\mathrm{Dy}}\mathbf{m}_i^{\mathrm{Dy}}], \quad j = 1, 2, \quad j \neq i. \quad (3)$$

Here, $\mathcal{H}_i^{\mathrm{CF(R)}}$ is the crystal field Hamiltonian, g_J^{R} is the Lande factor, $\mathbf{J}_i^{\mathrm{R}}$ is the angular momentum operator for the R ion, $g_S = 2$ is the g factor, $\mathbf{S}_i$ is the spin moment operator for the iron ion, and $\lambda_{\mathrm{fd}}^{\mathrm{R}} < 0$ and $\lambda < 0$ are the molecular constants of the R–Fe and Fe–Fe antiferromagnetic interactions.

The magnetic moments $\mathbf{M}_i^{\mathrm{Fe}}$ and $\mathbf{m}_i^{\mathrm{R}}$ of the ith iron and rare-earth sublattices per formula unit are defined, respectively, by the following relationships:

$$\mathbf{M}_i^{\mathrm{Fe}} = 3g_S\mu_B\langle\mathbf{S}_i\rangle, \quad \mathbf{m}_i^{\mathrm{R}} = g_J^{\mathrm{R}}\mu_B\langle\mathbf{J}_i^{\mathrm{R}}\rangle. \quad (4)$$

The right-hand side of the equation for $\mathbf{M}_i^{Fe}$ is the relevant Brillouin function, which is observed in the case of an equidistant spectrum of the Fe^{3+} ion for the thermal mean $\langle S_i \rangle$. The Fe^{3+} ion in $RFe_3(BO_3)_4$ is in the high-spin state [11], which gives the maximal value of the magnetic moment of the ion ($5\mu_B$).

The expression for a crystal field Hamiltonian $\mathcal{H}^{CF(R)}$ in irreducible tensor operators C_q^k has the form

$$\mathcal{H}^{CF(R)} = B_0^2 C_0^2 + B_0^4 C_0^4 + B_3^4 (C_{-3}^4 - C_3^4) + B_0^6 C_0^6 + B_3^6 (C_{-3}^6 - C_3^6) + B_6^6 (C_{-6}^6 + C_6^6). \quad (5)$$

The crystal field parameters B_q^k for the Nd^{3+} and Dy^{3+} ions in $Nd_{1-x}Dy_xFe_3(BO_3)_4$ are unknown. Exact information concerning the splitting of the ground multiplet of the Nd^{3+} and Dy^{3+} ions in $Nd_{1-x}Dy_xFe_3(BO_3)_4$ is not available either.

The computation of the values and orientations of the magnetic moments of the Fe and R subsystems in the self-consistent problems based on Hamiltonians (1)–(3) at the minimum of the corresponding thermodynamic potential makes it possible to determine the stability regions for various magnetic phases, phase-transition fields, magnetization curves, susceptibility, and so on. In the standard thermodynamic perturbation theory described in monograph [21] for *f–d* compounds, the thermodynamic potential can be written in the form

$$\Phi(T, B) = \frac{1}{2}\sum_{i=1}^{2}[-(1-x)k_B T \ln Z_i(\mathrm{Nd}) - xk_B T \ln Z_i(\mathrm{Dy}) + (1-x)\frac{1}{2}g_J^{Nd}\mu_B \langle \mathbf{J}_i^{Nd}\rangle \lambda_{fd}^{Nd}\mathbf{M}_i^{Fe} + x\frac{1}{2}g_J^{Dy}\mu_B \langle \mathbf{J}_i^{Dy}\rangle \lambda_{fd}^{Dy}\mathbf{M}_i^{Fe} - 3k_B T \ln Z_i(\mathrm{Fe}) + \frac{1}{2}3g_S\mu_B \langle \mathbf{S}_i\rangle (\lambda \mathbf{M}_j^{Fe} + (1-x)\lambda_{fd}^{Nd}\mathbf{m}_i^{Nd} + x\lambda_{fd}^{Dy}\mathbf{m}_i^{Dy}) + \Phi_{an}^i], \quad (6)$$

where $Z_i(R/Fe)$ are the partition functions calculated on Hamiltonians (1)–(3) and Φ_{an}^i is the anisotropy energy for the *i*th sublattice of the Fe system, which is much lower than the exchange energies and, hence, can be written as an additive term. For a crystal of trigonal symmetry, this energy has the form

$$\Phi_{an}^i = K_2 \cos^2 \vartheta_i + K_6 \sin^6 \vartheta_i \cos 6\varphi_i, \quad (7)$$

where $K_2 > 0$ is the uniaxial constant, $K_6 < 0$ is the anisotropy constant in the basal plane, and ϑ_i and φ_i are the polar and azimuth angles of the magnetic moment vector $\mathbf{M}_i^{Fe}$ for iron.

The magnetization and susceptibility of $Nd_{1-x}Dy_xFe_3(BO_3)_4$ are given by

$$\mathbf{M} = \frac{1}{2}\sum_{i=1}^{2}(\mathbf{M}_i^{Fe} + (1-x)\mathbf{m}_i^{Nd} + x\mathbf{m}_i^{Dy}), \quad \chi_k = \chi_k^{Fe} + (1-x)\chi_k^{Nd} + x\chi_k^{Dy}, \quad k = a, b, c. \quad (8)$$

In the ordered phase, the initial magnetic susceptibilities of the compound can be determined from the linear segments of the magnetization curves calculated for the corresponding directions of the external magnetic field. In the paramagnetic region, in which the interaction between the R and Fe subsystems can be disregarded, the magnetic susceptibility of the R subsystem can be calculated using the well-known Van Vleck formula, for which the energy spectrum and wavefunctions are calculated using crystal field Hamiltonian (5). The susceptibility χ_p^{Fe} of the Fe subsystem can be described by the Curie–Weiss law with the corresponding paramagnetic Néel temperature Θ:

$$\chi_p^{Fe} = \frac{\mu_{eff}^2}{3k_B(T-\Theta)}, \quad \mu_{eff}^2 = 105\mu_B^2 \text{ for } S = \frac{5}{2}. \quad (9)$$

The contribution of the R subsystem to the magnetic part of the specific heat of $Nd_{1-x}Dy_xFe_3(BO_3)_4$ compounds can be calculated using the conventional quantum-mechanical formula (per rare-earth ion, i.e., per formula unit):

$$C = (1-x)C_{Nd} + xC_{Dy}, \quad C_R = k_B\left(\frac{\langle E^2\rangle - \langle E\rangle^2}{(k_B T)^2}\right). \quad (10)$$

Thermal mean values $\langle E^2\rangle$ and $\langle E\rangle^2$ are calculated on the spectrum of the rare-earth ion, which is formed by the crystal field and by the interaction with the Fe subsystem and with the external magnetic field.

4. RESULTS AND DISCUSSION

To analyze the magnetic properties of $Nd_{1-x}Dy_xFe_3(BO_3)_4$ ferroborates theoretically, we must first determine the parameters of crystal field B_q^k because it is the crystal field that forms the electron structure of the rare-earth ion (its spectrum and wavefunctions) that makes a contribution to anisotropy of the magnetic properties of rare-earth ferroborates both in the paramagnetic and in the ordered temperature regions. To determine parameters of B_q^k, we used the experimental data for the temperature dependences of the initial magnetic susceptibility of $Nd_{1-x}Dy_xFe_3(BO_3)_4$ ($x = 0.15, 0.25$) along the trigonal axis in the basal plane in the paramagnetic regions

from $T_N \approx 31$ K to 300 K. For the initial crystal-field parameters from which the minimization procedure for the corresponding target function was launched, we used the parameters determined earlier in [9] for pure ferroborates $NdFe_3(BO_3)_4$ (for the Nd_{1-x} subsystem) and in [10] for $DyFe_3(BO_3)_4$ (for the Dy_x subsystem).

The resultant parameters, which strongly differed from the initial parameters, were rejected because the parameters of B_q^k for rare-earth compounds with a definite structure differ insignificantly in the rare-earth series. For each of the rejected set of parameters, we verified that susceptibilities $\chi_c(T)$ and $\chi_{\perp c}(T)$ in the paramagnetic region are described successfully; it was found that the paramagnetic Néel temperature for the Fe subsystems in the two compounds is approximately the same: $\Theta = -132$ K ($x = 0.15$) and $\Theta = -135$ ($x = 0.25$).

To find out which set of results parameters of B_q^k makes it possible to describe the entire aggregate of magnetic parameters of $Nd_{1-x}Dy_xFe_3(BO_3)_4$ ($x = 0.15$, 0.25), we calculated the magnetization curves along the trigonal axis and in the basal plane, $M_{c,\perp c}(B)$, to select parameters λ_{fd}^R (of antiferromagnetic Nd–Fe and Dy–Fe interactions) and λ_1 (of the Fe–Fe intrachain antiferromagnetic interaction). For the antiferromagnetic orientation of the magnetic moments of the Fe subsystem along the trigonal axis at $T < 4.2$ K and $\mathbf{B} \parallel \mathbf{c}$, the iron subsystem makes zero contribution to the magnetization in view of the smallness of the parallel susceptibility, and parameter λ_{fd}^R to which the magnetization curve is very sensitive in this region can be selected from the initial segment of the $M_c(B)$ curve. For $B > B_{SF}$ (B_{SF} is the field of the spin-flop transition), the slope of the magnetization curve is determined by the Fe–Fe intrachain exchange interaction λ_1 because the rotation of magnetization moments of iron in the flop phase towards the field direction occurs against the field. The resultant parameters λ_{fd}^R and λ_1 make it possible to calculate the $M_{c,\perp c}(B)$ curves at $T \le 4.2$ K. In this way, we determined several sets of crystal field parameters, which make it possible to most successfully describe the $\chi_{c,\perp c}(T)$ experimental susceptibility curves in the paramagnetic temperature range, as well as the $M_{c,\perp c}(B)$ magnetization curves.

The next important criterion for the final choice of parameters of B_q^k is the description of the temperature of the spontaneous spin-reorientation transition, $T_{SR} \approx 12.5$ K ($x = 0.15$) and $T_{SR} \approx 24$ K ($x = 0.25$). The calculations showed that this criterion imposes considerable limitations on the values of crystal field parameters. The spin-reorientation transition between the easy-axis and easy-plane states of $Nd_{1-x}Dy_xFe_3(BO_3)_4$ ($x = 0.15$, 0.25) is due to the competition between the contributions from the iron and rare-earth subsystems to the total magnetic anisotropy of the crystal. The magnetic anisotropy of the iron and neodymium subsystems stabilizes the easy-plane magnetic structure [2, 9]. The contribution from the dysprosium subsystem to the total anisotropy has the opposite sign and stabilizes the easy-axis structure [10]. Close values of different contributions to the total anisotropy of $Nd_{1-x}Dy_xFe_3(BO_3)_4$ ($x = 0.15$, 0.25) and their different temperature dependences lead to a spontaneous spin-reorientation transition.

Thus, following the above criteria of the description of the $\chi_{c,\perp c}(B)$ and $M_c(B)$ curves and the value of T_{SR}, from the entire set of crystal-field parameters determined at the initial stage we chose the sets that ensure the best description of experimental data for $Nd_{1-x}Dy_xFe_3(BO_3)_4$ ($x = 0.15$, 0.25) $\left(B_q^k[\mathrm{cm}^{-1}] = \frac{\mathrm{Nd[Dy]}(x=0.15)}{\mathrm{Nd[Dy]}(x=0.25)}\right)$:

$$B_0^2 = \frac{597[626]}{527[611]}, \quad B_0^4 = \frac{-1361[-1300]}{-1361[-1250]},$$
$$B_3^4 = \frac{750[-523]}{750[-623]}, \quad B_0^6 = \frac{585[696]}{585[696]}, \qquad (11)$$
$$B_3^6 = \frac{140[-60]}{140[-60]}, \quad B_6^6 = \frac{408[-283]}{420[-283]}.$$

These parameters were determined in calculations based on the ground multiplet; therefore, these parameters can be treated only as effective parameter that is suitable for describing the thermodynamic properties of the compound. It should be noted that parameters B_q^k for compositions with $x = 0.15$ and $x = 0.25$ are slightly different.

The set of parameters (11) corresponds to the values of energy of the eight lower levels of the ground multiplet of the Nd^{3+} and Dy^{3+} ions in $Nd_{0.75}Dy_{0.25}Fe_3(BO_3)_4$ given in Table 1 for $B = 0$. The values of energy are given for $T > T_N$ taking the f–d interaction at $T = 25$ K $> T_{SR}$ (easy-plane state) and $T = 2$, 23 K $< T_{SR}$ (easy-axis state) into account. Since parameters (11) for compositions with $x = 0.15$ and 0.25 differ insignificantly, the values of splitting Δ for $Nd_{0.85}Dy_{0.15}Fe_3(BO_3)_4$ are close. It can be seen from Table 1 that allowance for the f–d interaction at $T < T_N$ removes degeneracy; upon a decrease in temperature, splitting increases and the energy levels experience relative displacement at T_{SR}. In the case of Dy, the displacement of the energy levels increases splitting (from $\Delta = 0.9$ to 16.1 cm^{-1}), while for Nd, it leads to narrowing of the energy levels (from $\Delta = 11.6$ to 7.3 cm^{-1}).

The splitting of the ground multiplet of the Nd^{3+} and Dy^{3+} ions in $Nd_{1-x}Dy_xFe_3(BO_3)_4$ is determined by the joint action of the crystal field, external magnetic field $\mathbf{B}$, and the interaction with the iron subsystem. The position of the energy levels depends on

Table 1. Energy values for eight lower levels of the ground multiplet of the Nd^{3+} and Dy^{3+} ions in $Nd_{0.75}Dy_{0.25}Fe_3(BO_3)_4$, split by the crystal field (parameters (11)) and taking the *f–d* interaction for $B = 0$ into account in the paramagnetic and ordered temperature ranges

R	T	$\Delta = E_i - E_1$ ($i = 1$–8), cm^{-1}
Nd	$T > T_N$	0, 0, 79.2, 79.2, 165.8, 165.8, 261, 261
	25 K > T_{SR}	0, 11.6, 85.8, 85.9, 167, 176.6, 267, 267
	23 K < T_{SR}	0, 7.3, 73.5, 92.5, 163.8, 177.1, 256, 274
	2 K < T_{SR}	0, 8.2, 72.9, 94, 163.7, 178.5, 256, 276
Dy	$T > T_N$	0, 0, 21.9, 21.9, 108.6, 108.6, 207, 207
	25 K > T_{SR}	0, 0.9, 22.8, 23.7, 109.7, 109.7, 208, 208
	23 K < T_{SR}	0, 16.1, 23.3, 36.9, 110.7, 122.8, 206, 224
	2 K < T_{SR}	0, 17.8, 23.6, 38.5, 111, 124.3, 206, 226

the mutual orientation of the exchange and external fields acting on a rare-earth ion, as well as on their orientation relative to the principal crystallographic directions. Calculations show that the magnetic structure of $Nd_{1-x}Dy_xFe_3(BO_3)_4$ ($x = 0.15, 0.25$) at $T \approx T_{SR}$ is unstable; the rearrangement of the magnetic structure between the easy-axis and easy-plane states becomes possible. Thus, the situation in $Nd_{1-x}Dy_xFe_3(BO_3)_4$ ($x = 0.15, 0.25$) resembles that in the case of $HoFe_3(BO_3)_4$ [20]. The energy of the system can be lowered due to a change in the magnetic structure of the Fe subsystem (i.e., due to the change in the orientations of its magnetic moments from the easy-plane to the easy-axis state). The anisotropy energy of the iron and neodymium subsystems prevents such a change in the magnetic structure because these subsystems stabilize the easy-plane state. Upon a decrease in temperature, the possible gain in energy due to the transition from the easy-plane to the easy-axis structure increases and the system passes to the easy-axis state as a result of a first-order phase transition at T_{SR}. In the easy-axis phase, the energy levels of the ground multiplet of the Dy^{3+} ion exhibit the strongest splitting ($\Delta = 17.8\ cm^{-1}$). For the Nd^{3+} ion (whose contribution to the total anisotropy stabilizes the easy-plane state), the splitting is not maximal, but increases (from $\Delta = 7.3$ to $8.2\ cm^{-1}$). The population of the energy levels of the ground multiplet of the Nd^{3+} and Dy^{3+} is redistributed. This phenomenon is in fact a magnetic analog of the Jahn–Teller effect in rare-earth compounds (e.g., in RVO_4 with the zircon structure), in which an analogous redistribution of the population of energy levels occurs due to deformation of the crystal at low temperatures upon a change in the ground multiplet splitting; this effect is also accompanied by magnetic susceptibility anomalies (see, for example, [22]).

Further, using chosen parameters (11) of B_q^k, we calculated the $M_{c,\perp c}(B)$ magnetization curves in fields up to 9 T at temperatures corresponding to experimental values from 2 to 50 K and temperature dependences $\chi_{c,\perp c}(T)$ of the initial magnetic susceptibility in the temperature range from 2 to 300 K, as well as the contribution of the R subsystem to the specific heat of $Nd_{1-x}Dy_xFe_3(BO_3)_4$ ($x = 0$, 0.25, 1). Comparison with experimental data has made it possible to refine the parameters of $Nd_{1-x}Dy_xFe_3(BO_3)_4$ ($x = 0.15$, 0.25); for a unique set of parameters for each composition, we observed the conformity between the theory and experiment for the entire set of measured parameters.

It should be noted that an X-ray fluorescence analysis of the content of elements was carried out only for the compound with $x = 0.25$. In the solution–melt, we fixed concentration $x = 0.25$. Analysis showed that the concentration of Dy in $Nd_{0.75}Dy_{0.25}Fe_3(BO_3)_4$ was $x = 0.26 \pm 0.01$. Thus, the discrepancy between the preset and measured values of parameter x in $Nd_{0.75}Dy_{0.25}Fe_3(BO_3)_4$ was less than 5%. The calculations showed the best coincidence with experiment for $x_{calc} = 0.17$ and $x_{calc} = 0.266$ for compositions with $x = 0.15$ and 0.25, respectively.

The theoretical magnetic characteristics presented in the figures were calculated for parameters from Table 2, which also gives the parameters for pure ferroborates $NdFe_3(BO_3)_4$ from [9] and $DyFe_3(BO_3)_4$ from [10] for comparison. Parameter λ_2, which is given in Table 2 and appears in the Brillouin function, is responsible for the magnetic moment of iron at the given temperature and field and determines the Néel temperature because the 3D order in the ferroborate structure is impossible without the exchange interaction between the chains of Fe^{3+} ions. The value of parameter λ_2 was chosen from the condition of the best agreement between the experimental and calculated magnetization curves $M_{c,\perp c}(B)$ for all temperatures. In calculations, the uniaxial anisotropy constant $K_2 = 0.48\ T\ \mu_B$ for iron (at $T = 2$ K) and anisotropy constant $K_6 = -1.35 \times 10^{-2}\ T\ \mu_B$ for iron in the basal plane are also used.

Table 2 shows the difference in the values of molecular constant λ_{fd}^{Nd} for $Nd_{1-x}Dy_xFe_3(BO_3)_4$ ($x = 0.15$,

Table 2. Parameters of ferroborates $Nd_{1-x}Dy_xFe_3(BO_3)_4$ ($x = 0.15$, 0.25) studied here, as well as $NdFe_3(BO_3)_4$ and $DyFe_3(BO_3)_4$ from [9, 10]

Compound	$NdFe_3(BO_3)_4$	$Nd_{0.85}Dy_{0.15}Fe_3(BO_3)_4$	$Nd_{0.75}Dy_{0.25}Fe_3(BO_3)_4$	$DyFe_3(BO_3)_4$
$B_{dd1} = \lambda_1 M_0$, T	58	54	54	53
λ_1, T/μ_B	−3.87	−3.6	−3.6	−3.53
$B_{dd2} = \lambda_2 M_0$, T	27	30	28.5	28
λ_2, T/μ_B	−1.8	−2	−1.9	−1.87
$B_{fd} = \lambda_{fd}^R M_0$, T	7.1	11.5 (Nd) 2 (Dy)	11.5 (Nd) 2.3 (Dy)	3.3
λ_{fd}^R, T/μ_B	−0.47	−0.77 (Nd) −0.13 (Dy)	−0.77 (Nd) −0.15 (Dy)	−0.22
$\Delta_{fd} = \mu_B g\lvert\lambda_{fd}\rvert M_0$, cm^{-1}	8.8 (EP)	~8 (EA)Nd ~13 (EP)Nd ~15.7 (EA)Dy ~0.8 (EP)Dy	~8.2 (EA)Nd ~11.6 (EP)Nd ~17.8 (EA)Dy ~0.9 (EP)Dy	~19 (EA)
Θ, K	−130	−132	−135	−180

Note: B_{dd1} (intrachain Fe–Fe interaction), B_{dd2} (interchain Fe–Fe interaction), and B_{fd} are the low-temperature values of the exchange fields corresponding to molecular constants λ_1, λ_2, and λ_{fd}^R; Δ_{fd} is the low-temperature splitting of the ground state of the rare-earth ions due to the *f–d* interaction in the easy-axis (EA) and easy-plane (EP) states; Θ is the paramagnetic Néel temperature for the Fe subsystem; $M_0 = |M_i(T = 0, B = 0)| = 15\mu_B$ is the magnetic moment of iron per formula unit.

0.25) and $NdFe_3(BO_3)_4$, which can be explained by the difference in the low-temperature magnetic state (easy-plane state in $NdFe_3(BO_3)_4$ and easy-axis states in $Nd_{1-x}Dy_xFe_3(BO_3)_4$ ($x = 0.15$, 0.25)). It should also be noted that for easy-axis $PrFe_3(BO_3)_4$, which is close to $NdFe_3(BO_3)_4$ in the radius of the R ion, the value of parameter λ_{fd}^{Nd} is −0.73 T/μ_B [17], which is in conformity with the determined value of $\lambda_{fd}^{Nd} = -0.77$ T/μ_B (see Table 2).

We calculated the magnetic characteristics of $Nd_{1-x}Dy_xFe_3(BO_3)_4$ ($x = 0.15$, 0.25) for the external magnetic field directed along and across the trigonal axis taking the possible easy-axis and easy-plane states of the magnetic subsystem of the compounds into account using the diagrams of the orientation of magnetic moments $\mathbf{M}_i^{Fe}$ and $\mathbf{m}_i^R$ of iron and of the rare-earth elements depicted in Fig. 1. Calculations based on diagrams (a), (b), and (c) were performed for the magnetic-field direction along the trigonal axis ($\mathbf{B} \parallel \mathbf{c}$). Diagrams (d, e) were used for calculations for the field lying in the basal plane ($\mathbf{B} \perp \mathbf{c}$). The directions of the resultant magnetic moments $\mathbf{m}_1 = (1-x)\mathbf{m}_1^{Nd} + x\mathbf{m}_1^{Dy}$ and $\mathbf{m}_2 = (1-x)\mathbf{m}_2^{Nd} + x\mathbf{m}_2^{Dy}$ of the R subsystem, as well as their projections ($\mathbf{m}_{ic}$ and $\mathbf{m}_{ia}$) along the field, are indicated.

Experimental magnetization curves $M_c(B)$ presented in Fig. 2 for $Nd_{0.85}Dy_{0.15}Fe_3(BO_3)_4$ and in Fig. 3 for $Nd_{0.75}Dy_{0.25}Fe_3(BO_3)_4$ show that at $T = 2$ K the $M_c(B)$ curve exhibits a small jump in field $B \approx 1.1$ T ($x = 0.15$) and in field $B \approx 1.46$ T ($x = 0.25$), followed by a more pronounced magnetization jump at $B \approx 1.26$ T ($x = 0.15$) and $B \approx 1.66$ T ($x = 0.25$). Such a steplike form of the increase of the $M_c(B)$ curves with the field is also observed at other temperatures; with increasing temperature, the first jump becomes almost invisible at $T \approx 10$ K ($x = 0.15$) and $T \approx 16$ K ($x = 0.25$), while the second jump is distinguishable up to $T \approx 13$ K ($x = 0.15$) and $T \approx 23$ K ($x = 0.25$). The $M_c(B)$ curves for $T \geq 14$ K ($x = 0.15$) and $T \geq 24$ K ($x = 0.25$) increase monotonically. It should be noted that the distinguishable small anomaly, which is observed in weak field $B \approx 0.9$ T for $x = 0.15$, is absent on the $M_c(B)$ curves for $x = 0.25$ in weak fields.

Analysis of the experimental data, the results obtained in [4, 5, 7], and our calculations indicates that the magnetic moments of the Nd_{1-x}, Dy_x, and Fe subsystems in $Nd_{1-x}Dy_xFe_3(BO_3)_4$ ($x = 0.15$, 0.25) at low temperatures and $B = 0$ are oriented along the trigonal *c* axis (collinear phase, Fig. 1, diagram (a)). The sharp magnetization jump observed on the $M_c(B)$ curves in Figs. 2 and 3 is associated with the spin-flop transition from the initial collinear phase (Fig. 1, diagram (a)) to the flop phase (Fig. 1, diagram (b)) in the iron subsystem and is accompanied by reorientation of the magnetic moments of both sublattices of the Nd^{3+} and Dy^{3+} ions along field $\mathbf{B} \parallel \mathbf{c}$.

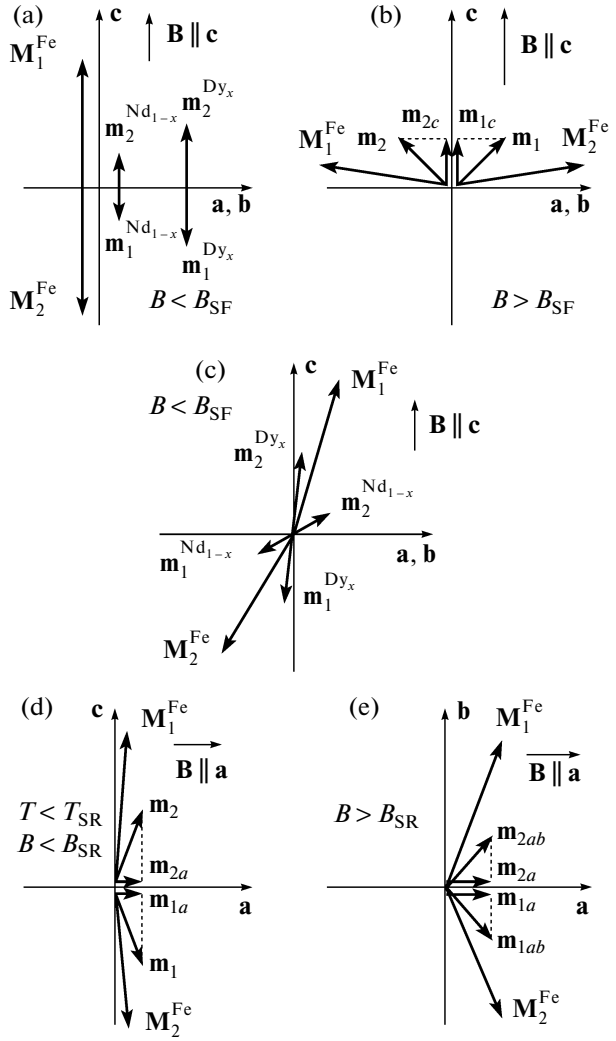

Fig. 1. Diagrams of orientation of magnetic moments $\mathbf{M}_i^{Fe}$ and $\mathbf{m}_i^{R}$ of iron and rare-earth element used for calculating the magnetic characteristics of $Nd_{1-x}Dy_xFe_3(BO_3)_4$ ($x = 0.15$, 0.25) for different temperature ranges and external magnetic field directions; $\mathbf{m}_{ic}$ and $\mathbf{m}_{ia}$ are the projections of the magnetic moments of the R subsystem along the field direction. Diagrams (a), (b), and (c) correspond to $\mathbf{B} \parallel \mathbf{c}$ (the *ab* plane is perpendicular to the plane of the figure). Diagrams for $\mathbf{B} \parallel \mathbf{a}$: (d) *ab* plane and the *b* axis is perpendicular to the plane of the figure; (e) the *c* axis is perpendicular to the plane of the figure.

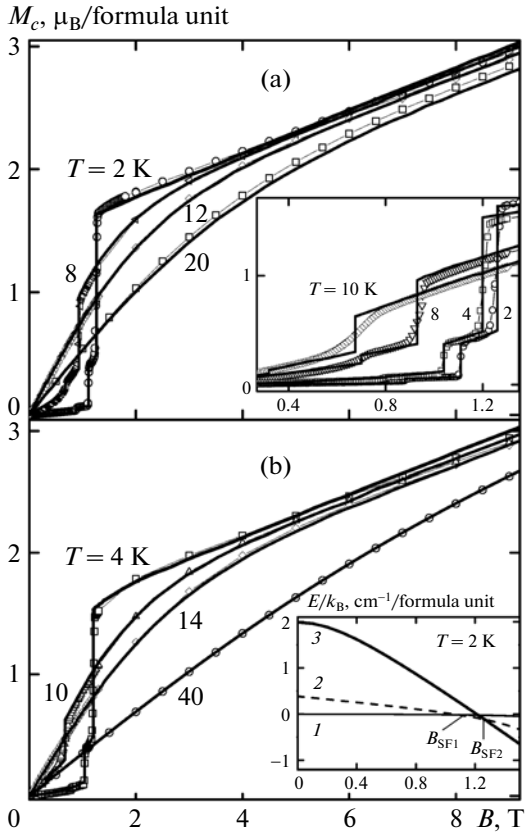

Fig. 2. Magnetization curves for $Nd_{0.85}Dy_{0.15}Fe_3(BO_3)_4$ for $\mathbf{B} \parallel \mathbf{c}$ at indicated temperatures. The symbols correspond to the experimental data and the curves correspond to theory. The inset to (a) shows the calculated and experimental magnetization curves for different temperatures in fields up to 1.5 T. The inset to (b) is the field dependence of the energies of $Nd_{0.85}Dy_{0.15}Fe_3(BO_3)_4$ in the easy-axis (curve *1*), intermediate (curve *2*), and easy-plane (curve *3*) states at $T = 2$ K and $\mathbf{B} \parallel \mathbf{c}$.

Detailed calculations of the magnetic phases that can be realized in $Nd_{1-x}Dy_xFe_3(BO_3)_4$ ($x = 0.15$, 0.25) for different orientations of the magnetic moments of the iron, neodymium, and dysprosium subsystems led to the assumption that the two-step form of the magnetization jump observed in Figs. 2 and 3 is probably due to the presence of an intermediate state between the collinear and flop phases. The first small jump on the $M_c(B)$ curves may be associated with a deviation of the magnetic moments of iron from the *c* axis through an angle on the order of 30° and with the formation of a weakly noncollinear antiferromagnetic phase (Fig. 1, diagram (c)). The second and more clearly manifested jump is due to reorientation of the magnetic moments of the Fe subsystem from the intermediate state (Fig 1, diagram (c)) to the flop phase (Fig. 1, diagram (b)) and is accompanied by reorientation of the magnetic moments of both sublattices of the Nd^{3+} and Dy^{3+} ions along the direction of field $\mathbf{B} \parallel \mathbf{c}$.

The reason for the formation of the possible intermediate state with a weakly noncollinear antiferromagnetic structure (Fig. 1, diagram (c)) is the competition between the contributions from the iron and neodymium subsystems to the total magnetic anisotropy of $Nd_{1-x}Dy_xFe_3(BO_3)_4$. The magnetic anisotropy of the iron and neodymium subsystems stabilizes the easy-plane magnetic structure, while the contribution from the dysprosium subsystem to the total anisotropy stabilizes the easy-axis structure. As a result, at certain values of temperature and magnetic

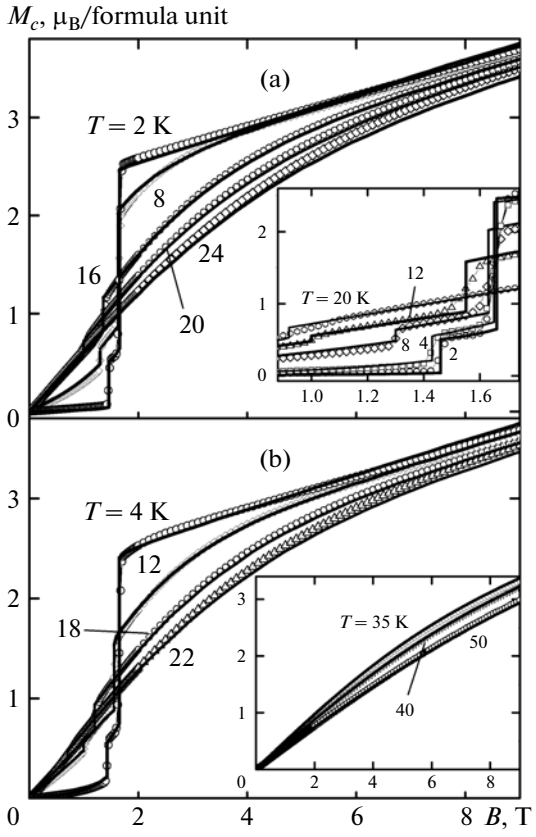

Fig. 3. Magnetization curves for $Nd_{0.75}Dy_{0.25}Fe_3(BO_3)_4$ for **B** || **c** at indicated temperatures. The symbols correspond to the experimental data and the curves correspond to theory. The insets show the calculated and experimental magnetization curves for different temperatures in fields up to 1.9 T (inset to (a)) and at $T > T_N$ (inset to (b)).

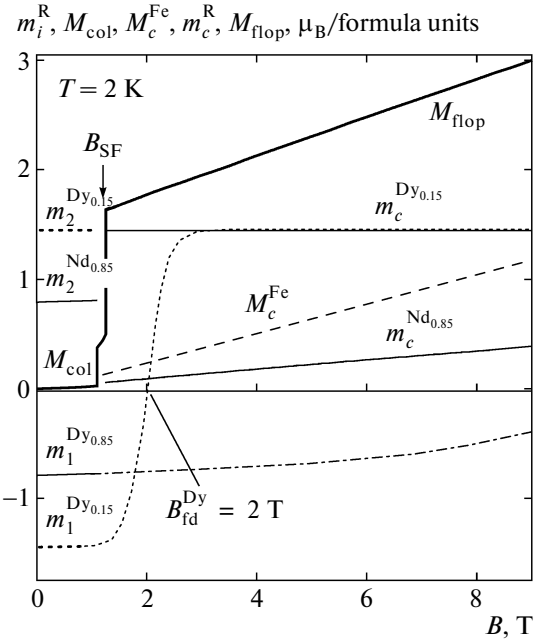

Fig. 4. Calculated field dependences of the magnetic moment components along the *c* axis for the R and Fe subsystems of $Nd_{0.85}Dy_{0.15}Fe_3(BO_3)_4$ in the collinear and flop phases at $T = 2$ K for **B** || **c**. Collinear phase ($B < B_{SF}$): $\mathbf{m}_1^R$ (magnetic moment is directed against the field) and $\mathbf{m}_2^R$ (along the field); M_{col} is the resultant magnetic moment in the collinear phase. Flop phase ($B > B_{SF}$): projections of moments $\mathbf{m}_c^R$ and M_c^{Fe} of the rare-earth and iron subsystems along the field; M_{flop} is the resultant magnetic moment in the flop phase.

field, the magnetic moments of iron can be oriented at an angle to the *c* axis; calculations show that these angles are different for compounds with $x = 0.15$ and $x = 0.25$. It should be noted that a conclusion about the deviation of the magnetic moments of iron from the *c* axis in the easy-axis phase through large angles, which are different at different temperatures and magnetic fields, was drawn earlier in [23] during study of $GdFe_3(BO_3)_4$, which also exhibits a spin-reorientation transition (see Fig. 6 in [23]).

Calculations based on diagram (c) in Fig. 1 allow us to explain the third small anomaly observed on the experimental $M_c(B)$ curve for $Nd_{0.85}Dy_{0.15}Fe_3(BO_3)_4$ at $T = 2$ and 4 K in field $B \approx 0.9$ T, assuming that a weakly noncollinear structure with a much smaller angle of deviation of the magnetic moments of iron from the *c* axis than for $B \approx 1.1$ T is formed in this field. The absence of the third low-field anomaly on the $M_c(B)$ curves for $x = 0.25$ is apparently associated with an increased contribution from the Dy subsystem, which stabilizes the initial state up to high fields.

The inset to Fig. 2b shows the field dependence of the energies of $Nd_{0.85}Dy_{0.15}Fe_3(BO_3)_4$ at $T = 2$ K in the easy-axis state (curve *1*), intermediate state in which the magnetic moments of the Fe subsystem are deflected from the *c* axis (curve *2*), and in the easy-plane state (curve *3*). Calculations show that for $B = 0$ and in fields up to 1.1 T, the easy-axis state (curve *1* and diagram (a) in Fig. 1) is the most advantageous state of the magnetic subsystem of $Nd_{0.85}Dy_{0.15}Fe_3(BO_3)_4$. Then, for $B_{SF1} \approx 1.1$ T, the intermediate state (curve *2* and diagram (c) in Fig. 1) becomes more advantageous and the weakly noncollinear antiferromagnetic structure makes a contribution to the first jump on the $M_c(B)$ curve. For $B_{SF2} \approx 1.26$ T, the flop phase (curve *3*, diagram (b) in Fig. 1) comes into play, in which the magnetic moments $\mathbf{m}_1^{Nd}$ and $\mathbf{m}_1^{Dy}$ of the neodymium and dysprosium subsystems are reoriented along the field, which makes the most significant contribution to the second magnetization jump on the $M_c(B)$ curve.

In the flop phase, the magnetic moments $\mathbf{M}_1^{Fe}$ and

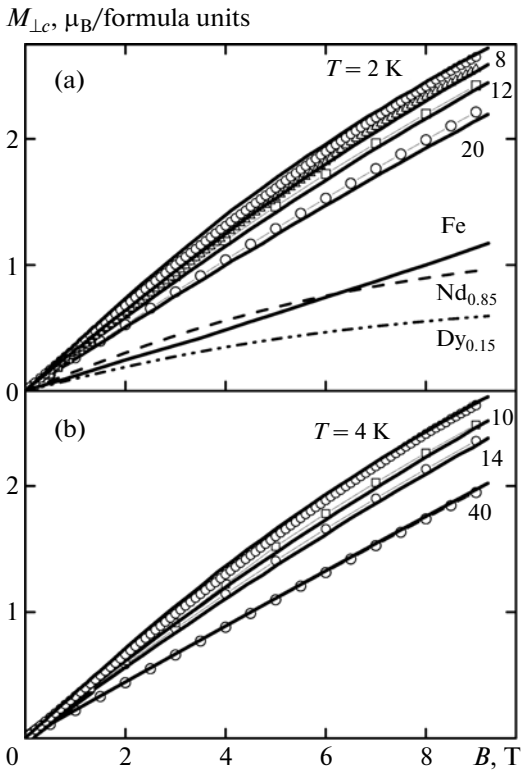

Fig. 5. Magnetization curves for $Nd_{0.85}Dy_{0.15}Fe_3(BO_3)_4$ for $\mathbf{B} \perp \mathbf{c}$ at indicated temperatures. The symbols correspond to the experimental data and the curves correspond to theory. Calculated contributions to the total magnetization from $Nd_{0.85}$, $Dy_{0.15}$, and Fe for $\mathbf{B} \perp \mathbf{c}$ at $T = 2$ K (a).

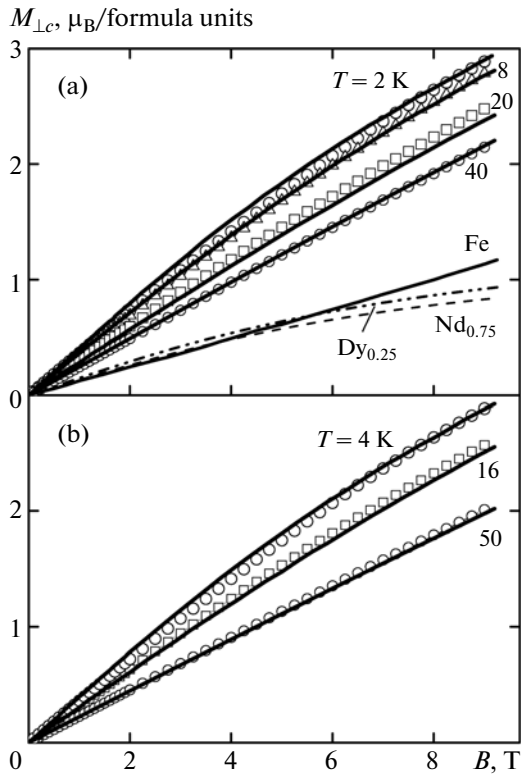

Fig. 6. Magnetization curves for $Nd_{0.75}Dy_{0.25}Fe_3(BO_3)_4$ for $\mathbf{B} \perp \mathbf{c}$ at indicated temperatures. The symbols correspond to experimental data and the curves correspond to theory. Calculated contributions to the total magnetization from $Nd_{0.75}$, $Dy_{0.25}$, and Fe for $\mathbf{B} \perp \mathbf{c}$ at $T = 2$ K (a).

$\mathbf{M}_2^{Fe}$ of the iron sublattices are bent towards the direction of field $\mathbf{B} \parallel \mathbf{c}$ and leave the *ab* plane.

The insets to Figs. 2a and 3a clearly show that the value of the spin-flop transition field B_{SF} decreases with increasing temperature (i.e., with increasing temperature, the initial collinear phase becomes less stable in spite of the increasing parallel susceptibility of the Fe subsystem). This $B_{SF}(T)$ dependence differs from those observed for $RFe_3(BO_3)_4$ with R = Pr [17], Nd [9], Tb [14], and Dy [10], for which the spin-flop transition field increases with temperature; this is usually observed in uniaxial antiferromagnets. An analogous behavior of the $B_{SF}(T)$ dependence, which was observed in $HoFe_3(BO_3)_4$ in [24, 25, 20], is due to the closeness of the temperatures at which the $M_c(B)$ curves were measured to temperature $T_{SR} \approx 12.5$ K of the spontaneous spin-reorientation transition (for $x = 0.15$) and $T_{SR} \approx 24$ K (for $x = 0.25$). Upon an increase in temperature, the overall effective anisotropy constant of the compound from the iron and rare-earth subsystems decreases.

In our calculations, the fields of the spin-flop transition for each temperature were determined from the equality of the thermodynamic potentials of the corresponding magnetic phases. It should be noted that the $M_c(B)$ magnetization curves in Figs. 2 and 3 were calculated for different values of the intrachain Fe–Fe exchange interaction parameter λ_1 in the collinear and flop phases. Thus, the situation with $Nd_{1-x}Dy_xFe_3(BO_3)_4$ ($x = 0.15$, 0.25) resembles that observed for $TbFe_3(BO_3)_4$ [13–15] and $DyFe_3(BO_3)_4$ [10]. For a correct description of the B–T phase diagram for $TbFe_3(BO_3)_4$, a slight (about 1%) difference in the values of exchange parameter λ_1 in the collinear and flop phases was assumed, which could be a consequence of the magnetoelastic effects accompanying this magnetic-field-induced first-order phase transition [13–15]. Subsequent calculations of the magnetoelastic effects in rare-earth ferroborates [17, 26, 27] revealed significant jumps in the multipole magnetic moments of the Tb^{3+} Ising ion in the ferroborate structure experiencing the spin-flop transition, which may lead to considerable jumps in the magnetostriction for this transition and, accordingly, to a change in the exchange parameter. The situation with $DyFe_3(BO_3)_4$ [10] differs from that in $TbFe_3(BO_3)_4$ in that the jumps of the multipole moments [16] of the anisotropic (and not Ising) Dy^{3+} ion in the spin-flop transition are smaller than for the Tb^{3+} ion; accordingly, the variation of the exchange parameter turned out to be smaller (about 0.1%) [10]. For $Nd_{0.75}Dy_{0.25}Fe_3(BO_3)_4$,

sharp magnetostriction jumps were observed in [4] in the spin-flop transition for $\mathbf{B} \parallel \mathbf{c}$. Calculations have shown that the difference in the values of exchange parameter λ_1 in the collinear and flop phases in $Nd_{1-x}Dy_xFe_3(BO_3)_4$ ($x = 0.15$, 0.25) is about 1.2%, which is in conformity with the experimental and calculated B–T phase diagrams.

It should be noted that anomalies on the experimental $M_c(B)$ magnetization curves associated with the spin-flop transition in $Nd_{0.75}Dy_{0.25}Fe_3(BO_3)_4$ differ from those given in [4], where only one anomaly is observed on the magnetization curves. The $Nd_{0.75}Dy_{0.25}Fe_3(BO_3)_4$ crystals on which our measurements were taken and those in [4, 5] were from the same growth experiment. Since a broad hysteresis loop was observed on the $M_c(B)$ curves in [4] for the spin-flop transition, one possible cause of the above difference may be the significant magnetocaloric effect and relaxation processes that occur in a magnetic system that is subjected to magnetization reversal in a pulsed field with a high rate of field application and removal. The emergence of a magnetic inhomogeneity in $Nd_{1-x}Dy_xFe_3(BO_3)_4$ ($x = 0.15$, 0.25) crystals, which is associated with the formation of regions with a predominance of Dy^{3+} or Nd^{3+} ions during crystal growth, is improbable for technological reasons. Magnetic measurements taken on samples of the same composition, but from different growth experiments, give coinciding results. The concentration inhomogeneity (namely, the difference in the concentrations of the Nd^{3+} and Dy^{3+} ions in the composition of growth pyramids for different faces of the crystal) was not measured. In all probability, the prepared samples contain regions that belong to different growth pyramids.

Figure 4 shows the field dependences of the magnetic moment components for the rare-earth and iron subsystems of $Nd_{0.85}Dy_{0.15}Fe_3(BO_3)_4$ along the c axis at $T = 2$ K for $\mathbf{B} \parallel \mathbf{c}$. Curves for $\mathbf{m}_1^{\mathrm{R}}$ and $\mathbf{m}_2^{\mathrm{R}}$ of the R sublattice with the magnetic moments directed against the field and along the field, the resultant magnetic moment $M_{\mathrm{col}} = m_2^{\mathrm{R}} - m_1^{\mathrm{R}}$ in the collinear phase (at $T = 2$ K and $\mathbf{B} \parallel \mathbf{c}$, the iron subsystem makes zero contribution to the magnetization), and resultant magnetic moment $M_{\mathrm{flop}} = M_c^{\mathrm{Fe}} + (1-x)m_c^{\mathrm{Nd}} + xm_c^{\mathrm{Dy}}$ in the flop phase are constructed as functions of the magnetic field.

Figure 4 clearly shows the difference in the values of M_{col} and M_{flop} in field B_{SF}, which is mainly due to the contribution from the R subsystem (the largest contribution comes from $Dy_{0.15}$) to the jump on the $M_c(B)$ curve in the given field. For $B = 0$, the magnetic moment is $m_2^{\mathrm{Nd}_{0.85}} = \left|m_1^{\mathrm{Nd}_{0.85}}\right| = 0.79\mu_{\mathrm{B}}$ ($m_2^{\mathrm{Nd}_{0.75}} = \left|m_1^{\mathrm{Nd}_{0.75}}\right| = 0.7\mu_{\mathrm{B}}$) for the neodymium subsystem and $m_2^{\mathrm{Dy}_{0.15}} = \left|m_1^{\mathrm{Dy}_{0.15}}\right| = 1.45\mu_{\mathrm{B}}$ ($m_2^{\mathrm{Dy}_{0.25}} = \left|m_1^{\mathrm{Dy}_{0.25}}\right| = 2.25\mu_{\mathrm{B}}$) for the dysprosium subsystem. In field $\mathbf{B} \parallel \mathbf{c}$ ($B = 2$ T), we have $m_a^{\mathrm{Nd}_{0.85}} = 1.24\mu_{\mathrm{B}}$ ($m_a^{\mathrm{Nd}_{0.75}} = 1.1\mu_{\mathrm{B}}$) and $m_c^{\mathrm{Nd}_{0.85}} = 0.091\mu_{\mathrm{B}}$ ($m_c^{\mathrm{Nd}_{0.75}} = 0.036\mu_{\mathrm{B}}$) for the neodymium subsystem and $m_a^{\mathrm{Dy}_{0.15}} = 0.19\mu_{\mathrm{B}}$ ($m_a^{\mathrm{Dy}_{0.25}} = 0.34\mu_{\mathrm{B}}$) and $m_c^{\mathrm{Dy}_{0.15}} = 1.44\mu_{\mathrm{B}}$ ($m_c^{\mathrm{Dy}_{0.25}} = 2.23\mu_{\mathrm{B}}$) for the dysprosium subsystem. Thus, after the spin-flop transition induced by field $\mathbf{B} \parallel \mathbf{c}$, the magnetic moments of the neodymium subsystem lie almost completely in the ab plane ($m_a^{\mathrm{Nd}_{1-x}} > m_c^{\mathrm{Nd}_{1-x}}$) due to a considerable f–d exchange ($\lambda_{\mathrm{fd}}^{\mathrm{Nd}} = -0.77$ Tl/μ_{B}), which ensures a small contribution to the magnetization $m_c^{\mathrm{Nd}_{1-x}}$ of the compound from the two neodymium sublattices (in particular, the magnetization jump on the theoretical $M_c(B)$ curve for B_{SF}.

For $\mathbf{B} \parallel \mathbf{c}$, the effective field acting on the rare-earth sublattice with magnetic moment $\mathbf{m}_1^{\mathrm{R}}$ directed oppositely to the external field decreases upon an increase in B and this magnetic moment tends to decrease (see Fig. 4). It is this process that determines the shape of the $M_c(B)$ curves at $T = 2$ K and $T = 4$ K up to spin-flop transition because at such a low temperature the Fe subsystem actually does not participate in the magnetization process due to the small parallel susceptibility ($T_N \approx 31$ K). Calculations show that this process is associated with the decrease in the splitting between the low energy levels of the Nd^{3+} and Dy^{3+} ions, which is determined by parameter $\lambda_{\mathrm{fd}}^{\mathrm{R}}$; for this reason, this segment on the magnetization curve is extremely sensitive to $\lambda_{\mathrm{fd}}^{\mathrm{R}}$. It is clear from Fig. 4 that with increasing field, the reorientation of the magnetic moments of the iron sublattices from the axis to the plane occurs before the vanishing of magnetic moments $\mathbf{m}_1^{\mathrm{Dy}_{0.85}}$ (fine dashed curve) and $\mathbf{m}_1^{\mathrm{Nd}_{0.15}}$ (fine dot-and-dash curve). This gives an estimate of the field exerted by the iron subsystem on the R subsystem (for $x = 0.15$): $B_{\mathrm{fd}}^{\mathrm{Nd}} \gg B_{\mathrm{SF}}(T = 2\ \mathrm{K}) \approx 1.1$ T and $B_{\mathrm{fd}}^{\mathrm{Dy}} > B_{\mathrm{SF}}(T = 2\ \mathrm{K}) \approx 1.26$ T. Processes analogous to those depicted in Fig. 4 also occur for the $Nd_{0.75}Dy_{0.25}Fe_3(BO_3)_4$ compounds.

For high fields in the basal plane, $Nd_{1-x}Dy_xFe_3(BO_3)_4$ ($x = 0.15$, 0.25) ferroborates are in the angular phase and behave as single-domain compounds, in which the magnetic moments of iron are bent to field $\mathbf{B} \perp \mathbf{c}$, exhibiting transverse susceptibility, which is independent of temperature for a typical antiferromagnet, while the magnetic moment components of the R subsystem parallel to the field increase (see diagram (e) in Fig. 1). Figures 5 and 6

show the experimental ($M_{\perp c}(B)$) and calculated ($M_a(B)$) magnetization curves in fields up to 9 T. It can be seen that the theoretical model proposed here provides a correct description of the behavior of the magnetization curves for $Nd_{1-x}Dy_xFe_3(BO_3)_4$ ($x = 0.15$, 0.25) in the basal plane and their temperature dependence, which is analogous to the experimental curve.

Let us consider the situation that occurs with magnetization of $Nd_{1-x}Dy_xFe_3(BO_3)_4$ ($x = 0.15$, 0.25) for $\mathbf{B} \perp \mathbf{c}$ in weak fields $B < 1$ T (for comparison with the experimental $M_{\perp c}(B)$ curves, we choose direction of $\mathbf{B} \parallel \mathbf{a}$). In accordance with the proposed theoretical model and analysis of the experimental data in field $B = 0$ for $T < T_{SR}$, $Nd_{1-x}Dy_xFe_3(BO_3)_4$ ($x = 0.15$, 0.25) ferroborates are in the easy-axis state and magnetic moments $\mathbf{M}_i^{Fe}$ and $\mathbf{m}_i^{R}$ of the iron and rare-earth subsystems are directed along the c axis; i.e., for the field direction $\mathbf{B} \perp \mathbf{c}$, the compounds are in the angular phase from the very outset (see diagram (d) in Fig. 1). Thus, it is possible to realize a spin-reorientation transition induced by field $\mathbf{B} \perp \mathbf{c}$, after which the magnetic moments of the Fe and R subsystems lie in the ab plane. In this phase, the magnetic moments of the Fe subsystem are rotated towards the field and the projection of magnetic moment $\mathbf{m}_i^{R}$ onto the field direction increases (diagram (e) in Fig. 1). In this case, the possible anomaly on the $M_{\perp c}(B)$ curves for the spin-reorientation transition induced by field $\mathbf{B} \perp \mathbf{c}$ is due to the difference between angular phase 1 (diagram (d) in Fig. 1) and angular phase 2 (diagram (e) in Fig. 1). It can be seen from Figs. 5 and 6 that the experimental $M_{\perp c}(B)$ curves do not exhibit appreciable anomalies; i.e., we can assume that the spin-reorientation transition induced by field $\mathbf{B} \perp \mathbf{c}$ is either absent or is not pronounced so that the projections of the magnetic moments along the field direction remain unchanged. The calculated $M_{\perp c}(B)$ curves in the case of the realization of field-induced reorientation transition do not exhibit appreciable anomalies in the critical field of the transition. It should be noted that such a weak manifestation of anomalies for the spin-reorientation transition induced by field $\mathbf{B} \perp \mathbf{c}$ was observed on the theoretical $M_a(B)$ curves, while anomalies in the experimental $M_a(B)$ curves for $HoFe_3(BO_3)_4$ are more pronounced [20, 24, 25]. The theoretical curves depicted in Figs. 5 and 6 were calculated using diagram (d) (see Fig. 1) for $T < T_{SR}$ and diagram (e) for $T > T_{SR}$ ($T_{SR} \approx 12.5$ K ($x = 0.15$) and $T_{SR} \approx 24$ K ($x = 0.25$)). Figures 5a and 6a show the components of the contribution to the magnetization at $T = 2$ K; comparison of these components indicates the extent of responsibility of each contribution to the resultant shape of the $M_{\perp c}(B)$ curve.

The contributions to the initial susceptibility of $Nd_{1-x}Dy_xFe_3(BO_3)_4$ come from the iron subsystem, which is ordered for $T < T_N$, and from the rate-earth (neodymium and dysprosium) subsystem magnetized

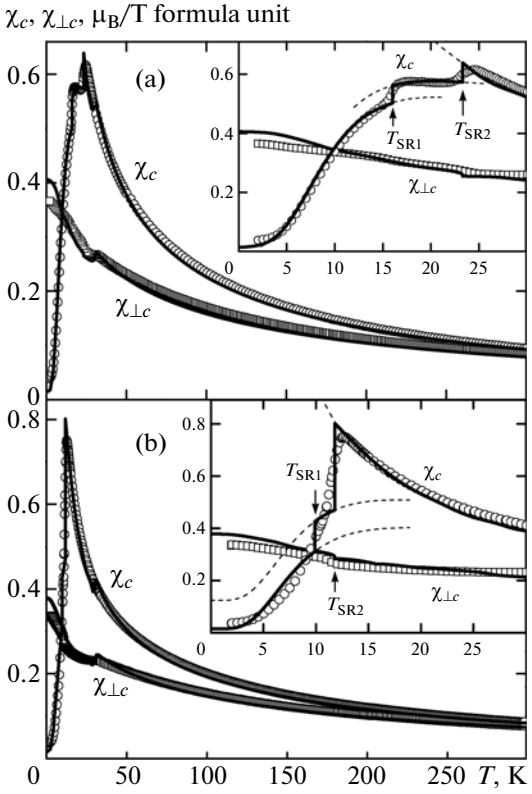

Fig. 7. Temperature dependences of the initial magnetic susceptibility of $Nd_{0.75}Dy_{0.25}Fe_3(BO_3)_4$ (a) and $Nd_{0.85}Dy_{0.15}Fe_3(BO_3)_4$ (b) for magnetic field directions $\mathbf{B} \parallel \mathbf{c}$ and $\mathbf{B} \perp \mathbf{c}$ for $B = 0.01$ T. The symbols correspond to the experimental data and the curves correspond to theory. The insets show the low-temperature range of the $\chi_{c,\perp c}(T)$ curves at $T < T_N$. Dashed curves show the predicted behavior of the $\chi_c(T)$ curves in the corresponding phases.

by the f–d interaction. Calculating these contributions self-consistently as described in Section 3, we obtain the temperature dependences $\chi_{c,\perp c}(T)$ of the initial susceptibilities shown in Fig. 7 for $Nd_{0.75}Dy_{0.25}Fe_3(BO_3)_4$ (a) and $Nd_{0.85}Dy_{0.15}Fe_3(BO_3)_4$ (b). The circles in the figures show experimental $\chi_{c,\perp c}(T)$ dependences. It can be seen that in the high-temperature regions from $T_N \approx 31$ to 300 K the theoretical curves correctly describe the experiment both for $x = 0.25$ (a) and for $x = 0.15$ (b). Calculations show that anisotropy of the $\chi_{c,\perp c}(T)$ curves in the paramagnetic temperature range is mainly due to the contribution from the dysprosium part of the rare-earth subsystem. The observed significant increase of the $\chi_{c,\perp c}(T)$ curves at $T < T_N$ is associated with the contribution from the R subsystem. An analogous increase in the $\chi_{c,\perp c}(T)$ curves at $T < T_N$ was also observed for $ErFe_3(BO_3)_4$ [18, 19] and $HoFe_3(BO_3)_4$ [20, 24, 25].

It can clearly be seen from Fig. 7 that anomalies on the experimental $\chi_c(T)$ curves, which correspond to the antiferromagnetic ordering in the Fe subsystem at $T_N \approx 31$ K, are almost indistinguishable. Upon a decrease in temperature, the experimental $\chi_c(T)$

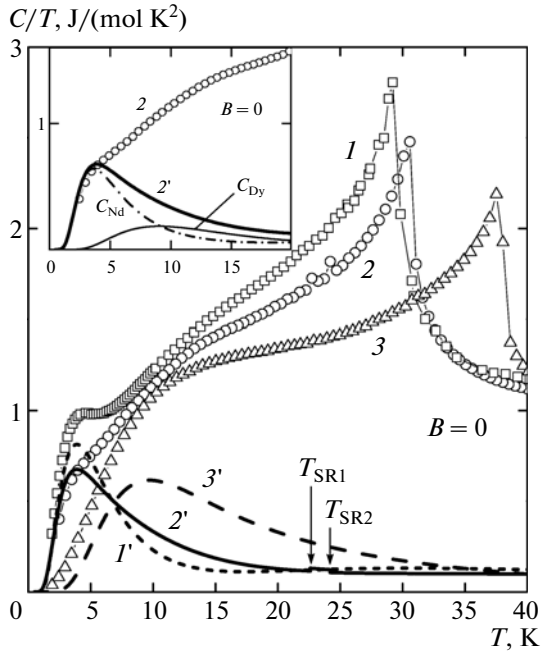

Fig. 8. Heat capacity of $NdFe_3(BO_3)_4$ (*1*), $Nd_{0.75}Dy_{0.25}Fe_3(BO_3)_4$ (*2*) and $DyFe_3(BO_3)_4$ (*3*) for $B = 0$ (curves *1* and *3* are plotted according to the data obtained in [28, 29]); curves show the calculated contribution of the R subsystem to heat capacity: $NdFe_3(BO_3)_4$ (dashed curve *1'*), $Nd_{0.75}Dy_{0.25}Fe_3(BO_3)_4$ (solid curve *2'*), and $DyFe_3(BO_3)_4$ (dot-and-dash curve *3'*). The inset shows the low-temperature region of the experimental and theoretical $C/T(T)$ curves (components of the R contribution are indicated) for $Nd_{0.75}Dy_{0.25}Fe_3(BO_3)_4$.

curves continue to increase, which is typical of the easy-plane state, while at $T \approx 24$ K (for $x = 0.25$ (a)) and $T \approx 12.5$ K (for $x = 0.15$ (b)), the $\chi_c(T)$ curves sharply descend, which can be explained by assuming the existence of a spin-reorientation transition from the easy-plane to the easy-axis state; this is confirmed by our calculations (solid curves in Fig. 7).

The insets to Figs. 7a and 7b show the low-temperature regions (for $T < T_N \approx 31$ K) of the experimental and theoretical $\chi_{c,\perp c}(T)$ dependences. Smoothed step anomalies on the experimental $\chi_c(T)$ curve for $Nd_{0.75}Dy_{0.25}Fe_3(BO_3)_4$ (a) at $T_1 \approx 16$ K and $T_2 \approx 24$ K can clearly be distinguished. For $Nd_{0.85}Dy_{0.15}Fe_3(BO_3)_4$ (inset to Fig. 7b), a relatively smooth decrease (without noticeable steps) can be observed on the experimental $\chi_c(T)$ curve at $T < T \approx 12.5$ K. It should be noted that step anomalies in $Nd_{0.75}Dy_{0.25}Fe_3(BO_3)_4$ analogous to those shown in Fig. 7a, which are weakly pronounced for 1 kOe and are clearly seen for 10 and 13 kOe, were also observed on the $\chi_c(T)$ curves from [4] (see Fig. 1b in [4]). Thus, in contrast to the $M_c(B)$ magnetization curves, the types of anomalies on our $\chi_c(T)$ curves for $Nd_{0.75}Dy_{0.25}Fe_3(BO_3)_4$ are the same as on the curves obtained in [4].

Our calculations and analysis of experimental data suggest that the step anomalies observed on the $\chi_c(T)$ curves for $Nd_{0.75}Dy_{0.25}Fe_3(BO_3)_4$ are due to the transition (upon an increase in temperature) from the easy-axis state to the easy-plane state, which occurs not as a single jump at T_{SR}, as in the case of $HoFe_3(BO_3)_4$ [20, 24, 25], but via an intermediate state formed at $T_{SR1} \approx 16$ K with the magnetic moments of the iron and rare-earth subsystems deflected from the *c* axis, followed by the easy-plane state formed at $T_{SR2} \approx 23.3$ K. As regards the low-temperature region on the experimental curves for $Nd_{0.85}Dy_{0.15}Fe_3(BO_3)_4$ (see the inset to Fig. 7b), in which there are no well-pronounced steps, the calculations in this case demonstrate a better coincidence with the experiment under the assumption that the reorientation of the magnetic moments of both sublattices of the Nd^{3+} and Dy^{3+} ions ($T_{SR2} \approx 11.8$ K) occurs after the formation of the intermediate angular phase at $T_{SR1} \approx 10$ K. The theoretical dashed $\chi_c(T)$ curves shown in the insets to Figs. 7a and 7b demonstrate the expected behavior of these dependences in the easy-axis, intermediate, and easy-plane states if the magnetic moments of the rare-earth and iron subsystems in $Nd_{1-x}Dy_xFe_3(BO_3)_4$ were not reoriented for calculated values of $T_{SR1} \approx 16$ K, $T_{SR2} \approx 24$ K (for $x = 0.25$ (a)) and $T_{SR1} \approx 10$ K, $T_{SR2} \approx 11.8$ K (for $x = 0.15$ (b)).

If the magnetic field lies in the basal plane, the temperature dependences of the initial magnetic susceptibility $\chi_{\perp c}(T)$ of $Nd_{0.75}Dy_{0.25}Fe_3(BO_3)_4$ (a) and $Nd_{0.85}Dy_{0.15}Fe_3(BO_3)_4$ (b) have anomalies near 24 K (a) and 11.8 K (b), which are associated with the spin-reorientation transition and are weakly pronounced on both the experimental and theoretical curves (Figs. 7a and 7b). The reorientation of the magnetic moments of all subsystems (from state (d) to state (e); see diagrams in Fig. 1) occurs with almost complete conservation of their projections along the field $\mathbf{B} \perp \mathbf{c}$.

It should be noted that for calculating the $\chi_{c,\perp c}(T)$ curves in the ordered temperature region, we used the parameters of the compounds determined from analysis of the field dependences of the $M_{c,\perp c}(B)$ magnetization curves; no fitting parameters were used.

The experimental data on the specific heat of $NdFe_3(BO_3)_4$ (curve *1* is plotted according to the data from [28]), $Nd_{0.75}Dy_{0.25}Fe_3(BO_3)_4$ (curve *2*), and $DyFe_3(BO_3)_4$ (curve *3* is plotted according to the data from [29]) for $B = 0$ are represented in Fig. 8 in the C/T vs. T coordinates. A clearly manifested peak on curve *1* at $T \approx 4.1$ K, less pronounced peaks near $T = 3.8$ K and $T = 13.4$ K on curve *2*, and a broad peak at $T \approx 10.6$ K on curve *3* are Schottky anomalies. Small sharp peaks, which can also be seen on curve *2* at $T = 22.6$ K and $T = 24.2$ K, are apparently associated with a spontaneous spin-reorientation transition from the easy-axis to the easy-plane state in $Nd_{0.75}Dy_{0.25}Fe_3(BO_3)_4$. It should be noted that the anomaly on the $C/T(T)$ curve associated with the spontaneous spin-reorientation transition in

$HoFe_3(BO_3)_4$ [20, 25] is manifested much more strongly. Figure 8 also shows the calculated contribution to the specific heat from the rare-earth subsystem of $NdFe_3(BO_3)_4$ (curve *1'* calculated with parameters from [9]), $Nd_{0.75}Dy_{0.25}Fe_3(BO_3)_4$ (curve *2'*), and $DyFe_3(BO_3)_4$ (curve *3'* calculated with the parameters from [10]). The contribution from the R subsystem to the specific heat of $Nd_{0.75}Dy_{0.25}Fe_3(BO_3)_4$ (curve *2'*) was calculated for the easy-axis state up to $T = 22.6$ K, in the intermediate state for 22.6 K $< T <$ 24.2 K, and in the easy-plane state for $T > T_{SR} \approx 24.2$ K. The inset to Fig. 8 shows the low-temperature region of the experimental and theoretical $C/T(T)$ curves for $Nd_{0.75}Dy_{0.25}Fe_3(BO_3)_4$. The calculated contribution from the R subsystem (curve *2'*) and the components of this contribution from the neodymium and dysprosium subsystems are also given in the figure.

It can be seen from Fig. 8 that the calculated contribution of the R subsystem to the specific heat of $Nd_{1-x}Dy_xFe_3(BO_3)_4$ ($x = 0$, 0.25, 1) compounds for $B = 0$ reproduces the experimental results. The low-temperature Schottky anomaly for $Nd_{0.75}Dy_{0.25}Fe_3(BO_3)_4$ (curves *2* and *2'*) is due to the contribution from the neodymium subsystem and is associated with the redistribution of the populations of the levels of the ground doublet of the Nd^{3+} ion split by the *f–d* interaction (see the inset to Fig. 8). The Schottky anomaly on experimental curve *2* near $T = 13.4$ K is due to the contribution from the dysprosium subsystem; it can be seen, however, that this anomaly becomes less pronounced on the overall theoretical curve *2'* due to allowance for the contribution from the neodymium part of the rare-earth subsystem as well.

Calculations show that if $Nd_{0.75}Dy_{0.25}Fe_3(BO_3)_4$ did not experience a spin-reorientation transition upon cooling, the Schottky anomaly for the easy-plane state would be near $T = 6.2$ K. The calculations performed for $Nd_{0.75}Dy_{0.25}Fe_3(BO_3)_4$ also predict a shift of the Schottky anomaly towards higher temperatures in increasing field $\mathbf{B} \parallel \mathbf{c}$.

5. CONCLUSIONS

We have experimentally and theoretically studied the magnetic properties of ferroborates with substituted compositions $Nd_{1-x}Dy_xFe_3(BO_3)_4$ ($x = 0.15$, 0.25) with competing Nd–Fe and Dy–Fe interactions and attained agreement between theory and experiment for the entire set of measured parameters. The unified theoretical approach based on the crystal field model for the rare-earth ion and in the molecular field approximation made it possible to determine parameters of $Nd_{1-x}Dy_xFe_3(BO_3)_4$ ($x = 0.15$, 0.25) ferroborates by comparing the results of calculations with experimental data. The values of determined parameters are comparable with the parameters for pure ferroborates with R = Nd and Dy (see Table 2).

Our calculations have shown that the spontaneous spin-reorientation transition observed for $Nd_{1-x}Dy_xFe_3(BO_3)_4$ ($x = 0.15$, 0.25) is a magnetic analog of the Jahn–Teller effect. The parameters determined in this study have allowed us to describe the experimental $M_{c,\perp c}(B)$ magnetization curves at various temperatures, as well as the experimental $B_{SF}(T)$ dependence; the critical field of the spin-flop transition decreases upon an increase in temperature due to a decrease in the overall effective anisotropy constant of the compound. For each composition, the spin-flop transitions observed at $T < T_{SR}$ in field $\mathbf{B} \parallel \mathbf{c}$ is described, and a possible version of explanation of the step anomalies on the $M_c(B)$ curves associated with this transitions is proposed.

We attained agreement between the experimental and theoretical $\chi_{c,\perp c}(T)$ temperature dependences in the paramagnetic temperature range at $\Theta = -132$ K ($x = 0.15$) and $\Theta = -135$ K ($x = 0.25$). Analysis of the competing contributions from the subsystems to the total anisotropy of $Nd_{1-x}Dy_xFe_3(BO_3)_4$ demonstrated the possibility of describing the observed anomalies on the $\chi_{c,\perp c}(T)$ curves below the Néel temperature. The calculated contribution from the R subsystem to the specific heat of $Nd_{1-x}Dy_xFe_3(BO_3)_4$ ($x = 0.15$, 0.25) for $B = 0$ reproduces the experimental results and clarifies the extent of responsibility of the components of the rare-earth contribution for the observed Schottky anomalies.

ACKNOWLEDGMENTS

The authors thank A.P. Pyatakov for fruitful discussions and his interest in this research.

This study was supported financially by the President of the Russian Federation (grant no. MK-497.2010.2).

REFERENCES

1. A. K. Zvezdin, S. S. Krotov, A. M. Kadomtseva, G. P. Vorob'ev, Yu. F. Popov, A. P. Pyatakov, L. N. Bezmaternykh, and E. A. Popova, JETP Lett. **81** (6), 272 (2005).
2. A. K. Zvezdin, G. P. Vorob'ev, A. M. Kadomtseva, Yu. F. Popov, A. P. Pyatakov, L. N. Bezmaternykh, A. V. Kuvardin, and E. A. Popova, JETP Lett. **83**, 509 (2006).
3. J. A. Campá, C. Cascales, E. Gutiérrez-Puebla, M. A. Monge, I. Rasines, and C. Ruíz-Valero, Chem. Mater. **9**, 237 (1997).
4. Yu. F. Popov, A. M. Kadomtseva, G. P. Vorob'ev, A. A. Mukhin, V. Yu. Ivanov, A. M. Kuz'menko, A. S. Prokhorov, L. N. Bezmaternykh, and V. L. Temerov, JETP Lett. **89** (7), 345 (2009).
5. I. A. Gudim, E. V. Eremin, and V. L. Temerov, J. Cryst. Growth **312**, 2427 (2010).
6. A. K. Zvezdin, A. M. Kadomtseva, Yu. F. Popov, G. P. Vorob'ev, A. P. Pyatakov, V. Yu. Ivanov, A. M. Kuz'menko, A. A. Mukhin, L. N. Bezmaternykh, and I. A. Gudim, JETP **109** (1), 68 (2009).

7. G. A. Zvyagina, K. R. Zhekov, I. V. Bilych, A. A. Zvyagin, L. N. Bezmaternykh, and I. A. Gudim, Low Temp. Phys. **36** (3), 279 (2010).
8. R. P. Chaudhury, F. Yen, B. Lorenz, Y. Y. Sun, L. N. Bezmaternykh, V. L. Temerov, and C. W. Chu, Phys. Rev. B: Condens. Matter **80**, 104424 (2009).
9. D. V. Volkov, A. A. Demidov, and N. P. Kolmakova, JETP **104** (6), 897 (2007).
10. D. V. Volkov, A. A. Demidov, and N. P. Kolmakova, JETP **106** (4), 723 (2008).
11. Y. Hinatsu, Y. Doi, K. Ito, M. Wakeshima, and A. Alemi, J. Solid State Chem. **172**, 438 (2003).
12. C. Cascales, C. Zaldo, U. Caldiño, J. García Solé, and Z. D. Luo, J. Phys.: Condens. Matter **13**, 8071 (2001).
13. E. A. Popova, D. V. Volkov, A. N. Vasil'ev, A. A. Demidov, N. P. Kolmakova, N. Tristan, and L. N. Bezmaternykh, in *Proceedings of the 34th Workshop on Low Temperature Physics (LT-34), Vardane, Krasnodar krai, Russia, September 26–30, 2006* (Rostov State Pedagogical University, Rostov-on-Don, Russia, 2006), Vol. 1, p. 78.
14. E. A. Popova, D. V. Volkov, A. N. Vasiliev, A. A. Demidov, N. P. Kolmakova, I. A. Gudim, L. N. Bezmaternykh, N. Tristan, Yu. Skourski, B. Büchner, C. Hess, and R. Klingeler, Phys. Rev. B: Condens. Matter **75**, 224413 (2007).
15. D. V. Volkov, E. A. Popova, N. P. Kolmakova, A. A. Demidov, N. Tristan, Yu. Skourski, B. Buechner, I. A. Gudim, and L. N. Bezmaternykh, J. Magn. Magn. Mater. **316**, e717 (2007).
16. D. V. Volkov and A. A. Demidov, in *Proceedings of the 35th Workshop on Low Temperature Physics (LT-35), Chernogolovka, Moscow oblast, September 29–October 2, 2009* (Chernogolovka, 2009), p. 158.
17. A. A. Demidov, N. P. Kolmakova, D. V. Volkov, and A. N. Vasiliev, Physica B **404**, 213 (2009).
18. D. V. Volkov and A. A. Demidov, in *Abstracts of Papers of the 5th International Conference on Functional Materials (ICFM-2009), Simferopol, Crimea, Ukraine, October 5–10, 2009* (Simferopol, 2009), p. 159.
19. D. V. Volkov and A. A. Demidov, Fazovye Perekhody, Uporyadochennye Sostoyaniya Novye Mater. **5**, 1 (2010).
20. A. A. Demidov and D. V. Volkov, Phys. Solid State **53** (5), 985 (2011).
21. A. K. Zvezdin, V. M. Matveev, A. A. Mukhin, and A. I. Popov, *Rare-Earth Ions in Magnetically Ordered Crystals* (Nauka, Moscow, 1985), p. 103 [in Russian].
22. G. A. Gehring and K. A. Gehring, Rep. Prog. Phys. **38**, 1 (1975).
23. S. A. Kharlamova, S. G. Ovchinnikov, A. D. Balaev, M. F. Thomas, I. S. Lyubutin, and A. G. Gavriliuk, JETP **101** (6), 1098 (2005).
24. C. Ritter, A. Vorotynov, A. Pankrats, G. Petrakovskii, V. Temerov, I. Gudim, and R. Szymczak, J. Phys.: Condens. Matter **20**, 365209 (2008).
25. A. Pankrats, G. Petrakovskii, A. Kartashev, E. Eremin, and V. Temerov, J. Phys.: Condens. Matter **21**, 436001 (2009).
26. A. A. Demidov, N. P. Kolmakova, L. V. Takunov, and D. V. Volkov, Physica B **398**, 78 (2007).
27. D. V. Volkov, A. A. Demidov, N. P. Kolmakova, and L. V. Takunov, Phys. Solid State **50** (9), 1677 (2008).
28. E. A. Popova, N. Tristan, C. Hess, R. Klingeler, B. Büchner, L. N. Bezmaternykh, V. L. Temerov, and A. N. Vasil'ev, JETP **105** (1), 105 (2007).
29. E. A. Popova, N. Tristan, and A. N. Vasiliev, Eur. Phys. J. B **62**, 123 (2008).

Translayed by N. Wadhwa